Nanotoxicology, 2011; Early Online, 1–12

ISSN: 1743-5390 print / 1743-5404 online
DOI: 10.3109/17435390.2011.606926

informa
healthcare

Nanoparticle inhalation alters systemic arteriolar vasoreactivity through sympathetic and cyclooxygenase-mediated pathways

Travis L. Knuckles[1,2], Jinghai Yi[1,2], David G. Frazer[2,4], Howard D. Leonard[4], Bean T. Chen[4], Vince Castranova[4], Timothy R. Nurkiewicz[1,2,3]

[1]*Center for Cardiovascular and Respiratory Sciences, West Virginia University School of Medicine, Morgantown, WV, USA,* [2]*Department of Physiology and Pharmacology, West Virginia University School of Medicine, Morgantown, WV, USA,* [3]*Department of Neurobiology and Anatomy, West Virginia University School of Medicine, Morgantown, WV, USA and* [4]*Pathology and Physiology Research Branch, Health Effects Laboratory Division, National Institute for Occupational Safety and Health, Morgantown, West Virginia, USA*

Abstract

The widespread increase in the production and use of nanomaterials has increased the potential for nanoparticle exposure; however, the biological effects of nanoparticle inhalation are poorly understood. Rats were exposed to nanosized titanium dioxide aerosols (10 μg lung burden); at 24 h post-exposure, the spinotrapezius muscle was prepared for intravital microscopy. Nanoparticle exposure did not alter perivascular nerve stimulation (PVNS)-induced arteriolar constriction under normal conditions; however, adrenergic receptor inhibition revealed a more robust effect. Nanoparticle inhalation reduced arteriolar dilation in response to active hyperaemia (AH). In both PVNS and AH experiments, nitric oxide synthase (NOS) inhibition affected only controls. Whereas cyclooxygenase (COX) inhibition only attenuated AH-induced arteriolar dilation in nanoparticle-exposed animals. This group displayed an enhanced U46619 constriction and attenuated iloprost-induced dilation. Collectively, these studies indicate that nanoparticle exposure reduces microvascular NO bioavailability and alters COX-mediated vasoreactivity. Furthermore, the enhanced adrenergic receptor sensitivity suggests an augmented sympathetic responsiveness.

Keywords: Microvascular, sympathetic nervous system, whole-body inhalation, nitric oxide, titanium dioxide

Introduction

Cardiovascular toxicity following inhalation of particulate matter (PM) is well established in the literature. General toxicity associated with PM exposure is enhanced as particle size decreases. As such, ultrafine particles and nanoparticles have been suggested to have an augmented toxicity compared with their larger counterparts (Stone et al. 2007). Nanotechnology is a burgeoning industry that is incorporated into our daily lives. Nanoparticles are classified as particles with a diameter of <100 nm in one dimension (Aitken et al. 2006) and have diverse applications in medical imaging, targeted drug delivery, anti-cancer therapy, as well as properties that are useful in the manufacturing of goods such as surface coatings, UV protectorates, among others (Aitken et al. 2006). However, without first properly identifying their potential for biological effects, the ubiquitous inclusion of these materials in everyday products significantly raises the risk of personal and occupational exposure that may be intentional or accidental. Nanotechnology has tremendous potential to contribute positively to society; however, for this to fully occur, the health effects of these materials must first be defined (Maynard et al. 2006).

Nano-TiO_2 is used in products such as photocatalysts (Sun et al. 2004), antibacterial surface coatings (Shieh et al. 2006), as well as in cosmetics and sunscreens (Aitken et al. 2006). These particles induce relatively minor levels of inflammation following pulmonary deposition, but nevertheless the biological effect is dose dependent (Nurkiewicz et al. 2008). Generally, inhalation of nano-TiO_2 results in diffuse alveolitis with some increases in phagocytic cell recruitment and oedema (Nurkiewicz et al. 2008). However, the pulmonary effects are relatively minor compared with other occupationally relevant particles such as residual oil fly ash (Dreher et al. 1997).

Based on a vast epidemiological, clinical and animal toxicology literature, three major hypotheses have been promoted to explain the remote cardiovascular effects following inhalation of particles. These are (1) particle translocation into the systemic circulation and direct particle–tissue interactions (Oberdorster et al. 2004), (2) systemic

Correspondence: Timothy R. Nurkiewicz, Department of Physiology & Pharmacology, Center for Cardiovascular and Respiratory Sciences, Robert C. Byrd Health Sciences Center, 1 Medical Center Drive, West Virginia University, Morgantown, WV 26506, USA. Tel: +304-293-7328. Fax: +(304) 293-5513. E-mail: tnurkiewicz@hsc.wvu.edu

(Received 11 February 2011; accepted 18 July 2011)

inflammation leading to peripheral effects (Tamagawa et al. 2008) and (3) alterations in autonomic nervous system (ANS) activity to elicit peripheral effects (Stone & Godleski 1999). While all three mechanisms may be important, the vast majority of investigations have focused on systemic inflammation. Indeed, our laboratory has previously demonstrated that inflammation-mediated microvascular dysfunction follows particle exposure (Nurkiewicz et al. 2004, 2006). However, efforts to re-establish normal microvascular function through depletion of peripheral neutrophils or elimination of oxidant stress have only been partially successful (Nurkiewicz et al. 2008, 2011).

The critical role of the microcirculation in maintaining homeostasis, particularly in vital organs such as the brain and heart, cannot be overstated. The arteriolar network is the principal site of vascular resistance. Reactivity at this level of the microvasculature to a host of influences maintains optimal perfusion through the capillary network to ensure adequate gas, nutrient and waste exchange for proper tissue and organ function. Furthermore, many diseases, such as hypertension, are microvascular in origin (Vicaut 1999). Hence, not only is the microcirculation important in maintaining homeostasis, but it is also, unfortunately, the origin of many pathological processes. Tissue perfusion at the microvascular level is regulated through a complementary (and sometimes redundant) system of intrinsic and extrinsic pathways. Arteriolar tone is the net result of their combined influences, and subtle changes in this active generation of arteriolar tone have profound influence on tissue perfusion. As such, altered responses to these vasoactive influences (or stimuli) can disturb tissue perfusion and, therefore, tissue homeostasis. Hence, the complex interplay between these intrinsic and extrinsic factors that control tissue perfusion is of paramount importance in regard to the systemic microvascular effects that follow nanoparticle exposure.

Arteriolar blood flow in skeletal muscle is controlled through the interplay between central (i.e. neural), hormonal and local mechanisms of blood flow control to achieve optimal capillary perfusion based on local metabolic demand (Segal 2005). At rest, perfusion is largely limited by sympathetic nerve activity, but during activity, it is increased, due to production and accumulation of vasoactive metabolites. These metabolites override the influence of sympathetic activity in arterioles inducing active hyperaemia (AH), which is an increase in blood flow that accompanies an increase in metabolic activity (Kurjiaka & Segal 1995; Segal 2005). However, blood flow can still be limited by sympathetic nerve activity, since metabolic influences induce vasodilation but do not eliminate sympathetic nerve activity (Kurjiaka & Segal 1995). Therefore, enhanced sympathetic tone can limit the ultimate metabolic capacity of a given tissue and therefore increase systemic blood pressure (Segal 2005).

Thus, the purpose of this study was to evaluate alternate pathways that may contribute to the microvascular dysfunction that follows nanoparticle inhalation and determine whether there is interaction between these pathways. Hence, our hypothesis is that the microvascular dysfunction associated with pulmonary nanoparticle exposure is not due entirely to endothelium-dependent mechanisms, but rather a dysfunction created by the combination of endothelium-dependent and endothelium-independent mechanisms.

Methods

Animals

Male Sprague Dawley rats (7–9 weeks old) were purchased from Hilltop Labs and housed in an Association for Assessment and Accreditation of Laboratory Animal Care International-approved animal facility at the National Institute for Occupational Safety and Health. Food and water were provided *ad libitum*. Additionally, male Sprague Dawley rats (7–9 weeks old) were purchased from Harlan Labs and housed in a PHS-approved animal facility at the West Virginia University Health Sciences Center. Because of animal housing restrictions, scheduling conflicts and facility resources, the control and nano-TiO_2 exposure groups contained a larger proportion of rats from either Hilltop Labs or Harlan Labs, respectively. As such, the animal vital statistics reflect a slight difference between the exposure groups (Table I). While these animals are of the same strain, these vendor-specific animals were delivered at slightly different ages, and because of vendor-specific growth curve differences, the age and weight statistics are different in Table I. However, our laboratory has previously shown that the microvascular reactivity is equivalent in male Sprague Dawley rats from these two vendors (Nurkiewicz et al. 2006). Furthermore, these groups, despite a slight difference in age, are both distinctly in the middle of a juvenile developmental stage (Linderman & Boegehold 1998). All animal procedures were performed on an approved protocol by the Institutional Animal Care and Use Committees at the National Institute for Occupational Safety and Health and West Virginia University.

Particles

The nano-TiO_2 powder was obtained from Degussa (Evonik, Aeroxide TiO_2, P25, primary particle size 21 nm, Parsippany, NJ). The powder was an approximate mixture of 80/20 of anatase/rutile (Nurkiewicz et al. 2008; Sager et al. 2008; Sager & Castranova 2009). The specific surface area of the particle was 48.08 m^2/g as measured by the BET gas absorption

Table I. Animal characteristics.

Experimental group	Animal number	Age (days)	Weight (g)	MAP (mm Hg)	SBP (mm Hg)	DBP (mm Hg)	HR (BPM)
Control	39	58 ± 1	241 ± 1	100 ± 1	121 ± 1	89 ± 1	359 ± 1
Nano-TiO_2	43	50 ± 1*	257 ± 1*	108 ± 1*	127 ± 1*	99 ± 1*	381 ± 1*

*$p < 0.05$ vs. control by ANOVA, Data ± SE.
DBP, diastolic blood pressure; HR, heart rate; MAP, mean arterial pressure; SBP, systolic blood pressure.

technique (Sager et al. 2008) The nano-TiO_2 powder was carefully prepared for generation by drying (to avoid agglomerate formation due to high humidity), sieving (to remove the large agglomerates) and storage (to prevent agglomerate attraction through contact charges) as previously described (Nurkiewicz et al. 2008).

Whole-body inhalation exposure

National institute for occupational safety and health

Aerosols were generated by a fluidised bed as previously described (Nurkiewicz et al. 2008). Briefly, animals were exposed to a 138 nm count geometric mean diameter particle (D_p) aerosol with a final concentration of 6 mg/m^3 of nano-TiO_2 for 4 h/day for 1 day. Real-time particle concentrations were monitored with a Data-RAM and confirmed gravimetrically with Teflon filters. This inhalation exposure concentration and duration has been shown previously to produce diffuse alveolitis with slight increases in phagocytic cell recruitment and oedema without producing overload (Nurkiewicz et al. 2008). Twenty-four h after nano-TiO_2 exposure, intravital microscopy was performed.

West virginia university

Nano-TiO_2 aerosols were generated with a vibrating fluidised bed, a Venturi vacuum pump and a cyclone separator (Figure 1) patent pending #61/455,355. The dry powder rested on a filter supported by a metal air distributor in the vibrating fluidised bed. The Venturi vacuum pump connected to the exit port of the fluidised bed has a high-velocity air jet blowing across a constriction in a pipe to create a suction that draws air and agglomerates of the particles into the Venturi vacuum pump. The large agglomerates were broken up by impaction and high-speed shear flow in the Venturi vacuum pump. After the Venturi vacuum pump, the aerosols enter a cyclone separator with a cut-off diameter of 400 nm at input flow rate of 60 l/min. Most large agglomerates were removed from the aerosol flow before entering the exposure chamber. The 0.5 m^3 exposure chamber (TSE, Bad Homburg, Germany) input air flow rate was 90 l/min with a pressure of −0.2 mbar. The animals were exposed 4 h/day for 1 day at a final concentration of 5.7 ± 0.25 mg/m^3 (Figure 2). The real-time size distribution and relative mass concentration of the particles in the chamber were monitored between 7 and 10,000 nm by an Electrical Low Pressure Impactor (ELPI, Dekati, Tampere, Finland) and the count mean aerodynamic diameter (D_{ae}) was determined to be 160 nm (Figure 3A). Frequency distribution of particle size based on number/cm^3 was derived from the ELPI data and overlaid with the actual particle number frequency distribution (Figure 3B). Real-time particle size distribution was also determined and between 14 and 670 nm (Figure 3C) by a Scanning Mobility Particle Sizer (SMPS, TSI, Shoreview, MN) and D_p was determined to be 160 nm. As above, frequency distribution of particle size based on number/cm^3 was derived from the SMPS data and overlaid with the actual particle number frequency distribution (Figure 3D). These frequency distributions allow data above the 670 nm cut-off of the SMPS assumed based on a presumed normal distribution. The particle mass concentrations were confirmed gravimetrically with Teflon filters. A calculated total pulmonary deposition was estimated to be 30 μg using both steady-state nanoparticle concentration and area under the curve. Our exposure calculation were made and rounded to be conservative. After twenty-four hours post-exposure, this concentration of nano-TiO_2 yields a total measured pulmonary deposition of 10 μg (Nurkiewicz et al. 2008).

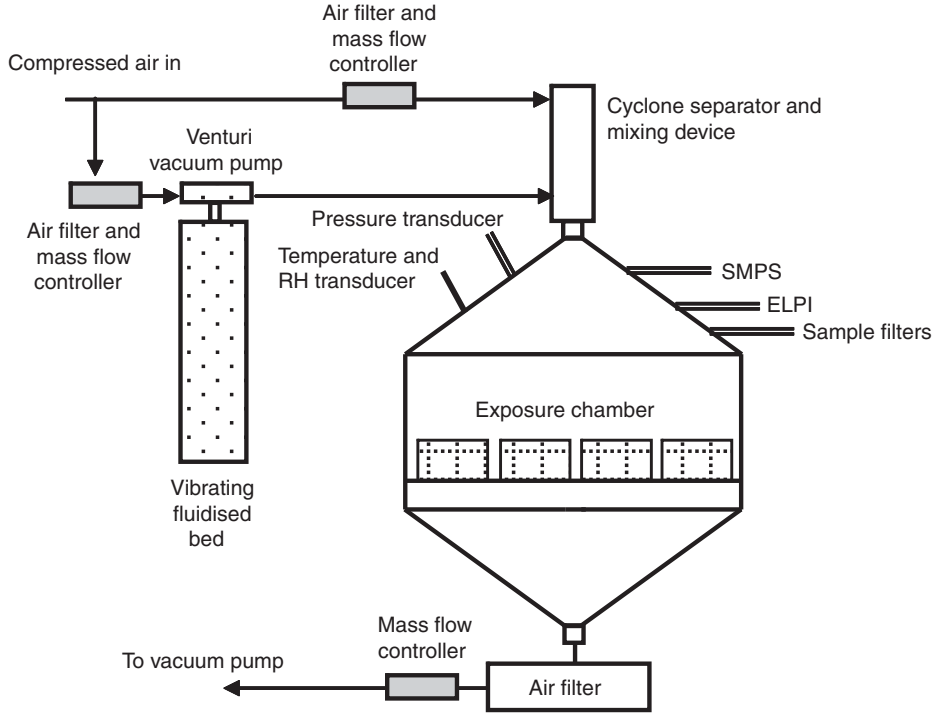

Figure 1. West Virginia University inhalation exposure facility schematic for the generation of nano-TiO_2 aerosols.

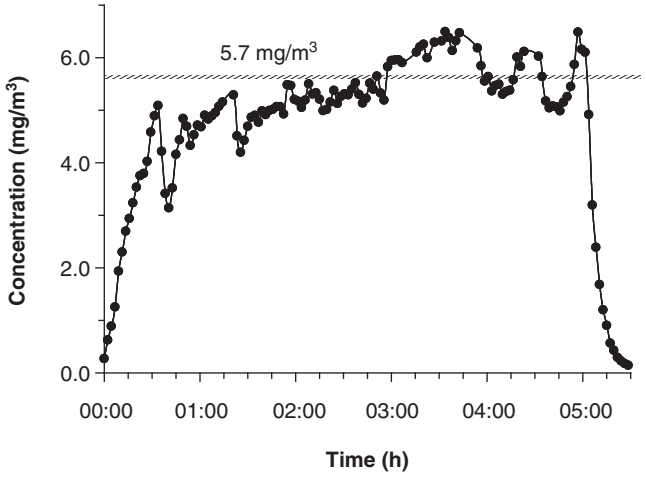

Figure 2. Real-time nano-TiO_2 concentrations over the exposure period. Dots represent 2-min averages with an average particle concentration of 5.7 mg/m^3.

Particle sizes and concentrations used in the two exposure environments were slightly different; however, the particle composition and estimated dose were the same. As such, the results from these two exposures were similarly interpreted.

Intravital microscopy

Intravital microscopy was performed as previously described (Nurkiewicz et al. 2004). Rats were anesthetised by an i.p. injection of sodium thiopental (100 mg/kg) and placed on a heating pad to maintain a rectal temperature of 37°C. The trachea was intubated to ensure a patent airway, and the right carotid artery was cannulated to measure arterial pressure. The right spinotrapezius muscle was exteriorised for microscopic observation, leaving feed vessels and innervation intact. The muscle was then gently secured over a clear pedestal at its *in situ* length and enclosed in a tissue bath and continuously superfused with an electrolyte solution (119 mM NaCl, 25 mM $NaHCO_3$, 6 mM KCl and 3.6 mM $CaCl_2$, pH 7.4, 290 mOsm), warmed to 35°C and equilibrated with 95% N_2, 5% CO_2. Superfusion flow rate was maintained at 4–6 ml/min to minimise equilibration with atmospheric oxygen (Boegehold & Bohlen 1988). The preparation was then transferred to the stage of an Olympus intravital microscope (Model BX51WI, Center Valley, PA) coupled to a CCD camera (Olympus Model DP71) and was observed under a 20X water immersion objective (final image magnification was 743X.). One to three arcade bridge arterioles were studied per animal preparation. These arterioles are the

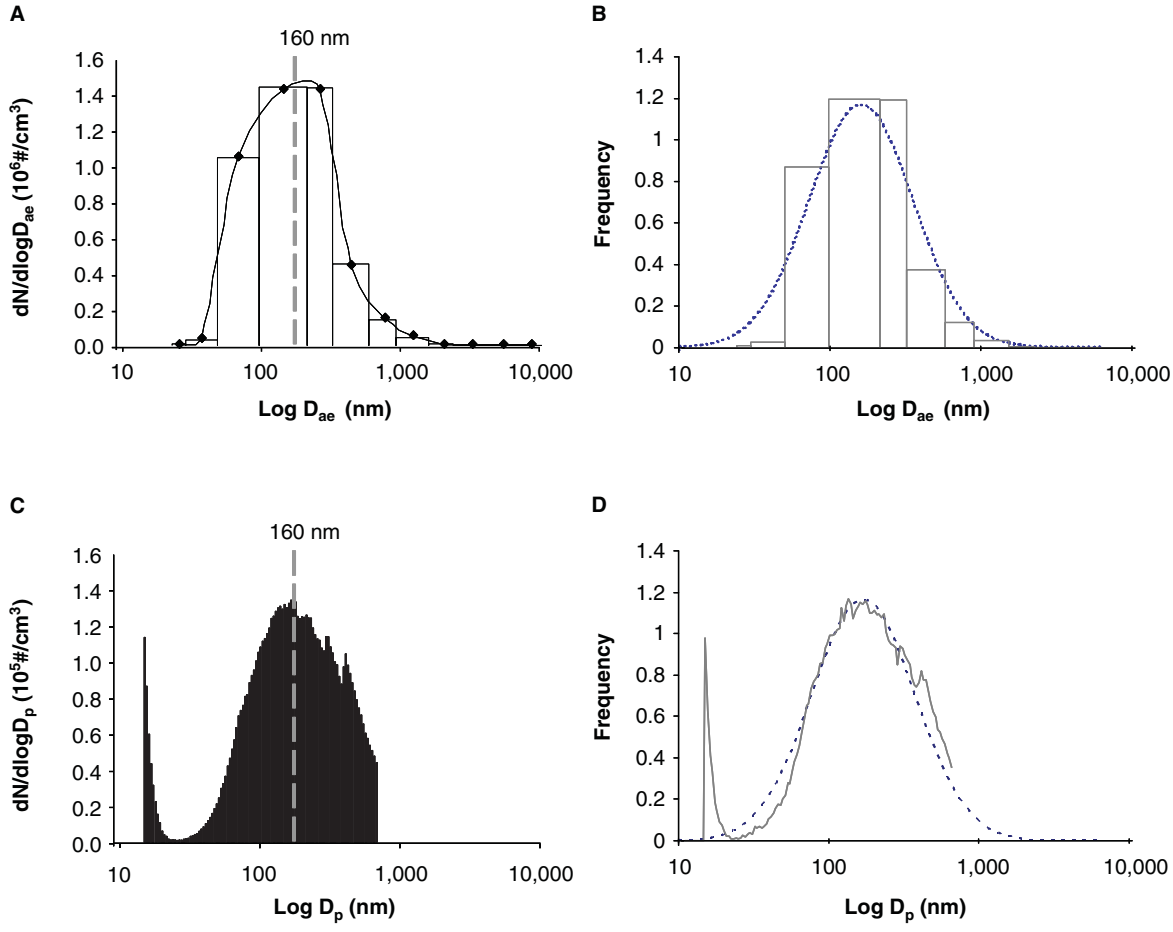

Figure 3. Nano-TiO_2 particle size distribution. (A) Representative ELPI size distribution of the nano-TiO_2 aerosol for the 13 impactor stages (between 7 and 10,000 nm). Average nano-TiO_2 aerosol count median aerodynamic diameter (D_{ae}) was 161 nm. (B) Gaussian distribution of particle size based on frequency. The dotted line is the model fit for a lognormal distribution function with a median (or geometric mean) of 160 nm and a geometric standard deviation of 2.2. The lighter grey line is the actual data from the ELPI. (C) Representative SMPS size distribution curve for the nano-TiO_2 aerosol over the 107 size cut-offs (between 14 and 670 nm). Average nano-TiO_2 aerosol count geometric mean diameter (D_p) was 159 nm. (D) The dotted line is the model fit for a lognormal distribution function with a median (or geometric mean) of 160 nm and a geometric standard deviation of 2.2. The solid lighter grey line is the actual data from the SMPS.

site of the majority of vascular resistance in the spinotrapezius muscle and hence of major importance in regulation of blood flow in the muscle (Boegehold 1991). The arcade bridge arteriole originates from the thoracodorsal and 11th intercostal arteries at the proximal and distal ends, respectively, of the muscle forming a loop that contributes the entire blood supply for the arcading vascular network (Schmid-Schonbein et al. 1991). Real-time images were displayed on a high-resolution computer monitor. Greater than three images were digitally captured via DP Controller (Olympus, Center Valley, PA) during a baseline period and immediately following each experimental period. Arteriolar diameters from each digital image were determined by Microsuite analysis software (Olympus, Center Valley, PA) calibrated with a stage micrometer. Arteriolar diameters were averaged per experimental end point to reduce sampling variability.

Superfusate chemicals

Compounds were introduced via a syringe pump at 1/10 of the flow rate (i.e. 0.4–0.6 ml/min). N^G-monomethyl-l-arginine (L-NMMA, Calbiochem, Gibbstown, NJ) was used at a final tissue bath concentration of 100 μM to inhibit NOS activity (Nase & Boegehold 1997a; Linderman & Boegehold 1998). Meclofenamate (MEC, Sigma-Aldrich, St. Louis, MO) was used at a final concentration of 30 μM to inhibit COX activity (Nase & Boegehold 1997b; Linderman & Boegehold 1998). The final tissue bath concentration of phentolamine (Sigma-Aldrich, St. Louis, MO), an α-adrenergic receptor blocker (Kurjiaka & Segal 1995; Nase & Boegehold 1997b; Linderman & Boegehold 1998), and tetrodotoxin (Sigma-Aldrich, St. Louis, MO) (Kurjiaka & Segal 1995; Linderman & Boegehold 1998), a fast sodium channel blocker that inhibits all nerve function, was 1 μM. Superfusate concentrations of these inhibitors have been previously shown to be effective in the spinotrapezius muscle preparation (Kurjiaka & Segal 1995; Lash 1995; Nase & Boegehold 1997b; Linderman & Boegehold 1998; Marvar et al. 2005). U46619 and iloprost (Cayman Chemical, Ann Arbor MI) were superfused at a final concentration of 1–100 nM or 2.8–28 nM, respectively (Didion et al. 1997; Xiang et al. 2006). Adenosine (ADO, Sigma-Aldrich, St Louis, MO) was superfused at the end of the experiments (100 μM) to determine passive arteriolar diameters.

Statistics

Arteriolar diameter (D, in micrometres) was recorded during a control or perivascular nerve stimulation (PVNS) period and immediately following AH or during superfusion with pharmacological agents. Resting vascular tone was calculated for each vessel as follows: tone = $[(D_{pass} - D_c)/D_{pass}]\bullet 100$, where D_{pass} is passive diameter under ADO and D_c is the diameter measured during the control period. A tone of 100% represents complete vessel closure, whereas 0% represents the passive state. Arteriolar responses were normalised as follows: percent change from control = $[(D_{ss}/D_c) - 1]\bullet 100$, where D_{ss} is the steady-state diameter following AH and PVNS or during tissue superfusion. All data are reported as mean ± SE. Statistical analyses were performed with commercially available software (Sigmastat; Chicago, IL). Two-way repeated measures ANOVA was used to determine the effects of group, treatment and group–treatment interactions on measured variables. For all ANOVA procedures, the Student–Newman–Keuls post-hoc analysis was used to identify pair-wise differences among specific groups. Significance was assessed at the 95% confidence level ($p < 0.05$) for all tests.

Experimental protocols

Protocol 1

PVNS was performed on arcade bridge arterioles to determine responsiveness to sympathetic nerve stimulation. To accomplish this, a bevelled micropipette was filled with 0.9% saline and attached to a Grass current programmer. The tip of the micropipette was brought to gently rest in the adventitia of the arteriole to be studied. The perivascular nerves were stimulated for 20–60 sec to develop stable constriction at a randomly assigned frequency of 2, 4, 8 or 16 Hz. This stimulation protocol has been previously demonstrated to produce stable vasoconstriction without inducing escape during the stimulation period (Kurjiaka & Segal 1995). The observation site was distal to the stimulation site by 2–5 mm in the direction of flow to ensure that the effects of stimulation were neural in origin and not from depolarisation of the vascular smooth muscle cells, as previously described (Kurjiaka & Segal 1995; Linderman & Boegehold 1998). Microvascular reactivity was assessed first under normal superfusate conditions, then in the presence of L-NMMA, MEC, phentolamine or tetrodotoxin. Arterioles were allowed to recover a minimum of 2 min between stimulations to return to baseline diameters following each randomly assigned frequency.

Protocol 2

AH was induced in a separate set of rats through the stimulation of muscular contraction to determine the impact of nanoparticle exposure on metabolically induced vasodilation. To induce muscular contraction, electrodes were attached to the rostral and caudal ends of the spinotrapezius muscle to stimulate the muscle at 2, 4, 8 and 12 Hz at 0.2 msec in duration at 3–6 V for 1 min as previously described (Lash & Bohlen 1987). Voltage was determined empirically for each animal preparation to produce the maximum contraction in the muscle (Lash & Bohlen 1987). Variables that influenced voltage were primarily animal weight and muscle length. Most of our experiments were conducted at 5V. The frequencies used in the protocol have been shown to be below the threshold for direct excitation of vascular smooth muscle or autonomic neurons as well as being non-tetanic (Lash & Bohlen 1987). Frequencies 2–8 Hz are physiologically relevant with the supraphysiological stimulation of 12 Hz performed to maximally produce vasoactive metabolites (Lash & Bohlen 1987). Superfusate inhibitors (L-NMMA, MEC and phentolamine) were added following normal superfusate responses to determine mechanistic changes in microvascular reactivity. Tetrodotoxin was not evaluated since at 1 μM the compound at this concentration inhibits normal skeletal muscle contraction. Arterioles were

allowed to recover a minimum of 2 min between stimulations to return to baseline diameter following each randomly assigned frequency.

Protocol 3

A separate set of rats were prepared for intravital microscopy. Baseline images were collected for each arcade bridge arteriole studied, and then the muscle was superfused with either U46619 or iloprost for 10 min per dose. Following each randomly assigned dose, images of each arcade bridge arteriole were taken and the microvascular network was allowed to recover and return to baseline for at least 10 min following each dose. Following all protocols and at the end of the experiment, the muscle was superfused with ADO for 10 min to determine D_{pass}.

Results

Microvessel characteristics

Arteriolar diameter and tone under normal superfusate conditions were not different between control and nano-TiO_2-exposed animals (Table II). The various superfusate treatments did not alter arteriolar diameter or tone except for phentolamine treatment in the nano-TiO_2-exposed group. Superfusion with this α-adrenergic antagonist significantly increased arteriolar diameter and reduced tone only in the nanoparticle-exposed group (Table II).

Nanoparticle exposure alters response to α-adrenergic stimulation

To determine whether nanoparticle exposure augments the influence of the sympathetic nervous system on arteriolar constriction, perivascular nerves associated with arcade bridge arterioles were stimulated in control and nano-TiO_2-exposed animals (Figure 4). Under the normal superfusate, nanoparticle exposure did not appear to alter perivascular nerve-mediated constriction (max −36% +/− 3 control, −32% +/− 2 nano-TiO_2, 16 Hz (Figure 4A)). However, inhibition of NOS via L-NMMA superfusion enhanced arteriolar constriction in control animals but did not alter this constriction in nano-TiO_2-exposed animals (−57% +/− 5 control, −39% +/− 7 nano-TiO_2, 16 Hz (Figure 4B)). Arteriolar constriction was overtly blunted with α-adrenergic blockade in both the nano-TiO_2-exposed animals and control animals at 8 and 16 Hz compared with the normal superfusate treatment (max response −24% +/− 6 control, −9% +/− 2 nano-TiO_2 (Figure 4C)). Nano-TiO_2 exposure increased sensitivity to α-adrenergic blockade compared with control arterioles at 8 and 16 Hz (Figure 4C). Ablation of all nerve activity with tetrodotoxin rendered arteriolar reactivity to PVNS unresponsive in both the groups (Figure 4D). All frequency modulations for both control and nano-TiO_2-exposed animals superfused with tetrodotoxin were significantly different from the respective normal superfusate equivalents (Figure 4D), suggesting pharmacological ablation of nerve function completely disrupts changes in PVNS-induced arteriolar constriction. Arteriolar dilation induced by PVNS in the presence of tetrodotoxin, which has been demonstrated previously (Linderman & Boegehold 1998), was not different between control and nano-TiO_2-exposed animals. Inhibition of COX, via MEC superfusion, did not alter responses in control or nano-TiO_2-exposed animals (data not shown).

Nanoparticle exposure blunts active hyperaemia

Spinotrapezius muscle arteriolar responses to increased metabolic demand were frequency dependent (Figure 5). Exposure to nano-TiO_2 particles significantly reduced vasodilation at 12 Hz compared with control animals (max 183% +/− 13 control, 144% +/− 15 nano-TiO_2 (Figure 5A)). The addition of an NOS inhibitor significantly blunted vasodilation in the control animals but not in nano-TiO_2-exposed animals at 8 and 12 Hz (max 61% +/− 12 control, 152% +/− 17 nano-TiO_2 (Figure 5B)), suggesting a reduction in NO bioavailability in the nano-TiO_2-exposed animals. Inhibition of COX with MEC significantly reduced arteriolar dilation in nano-TiO_2-exposed animals at 8 and 12 Hz while not altering dilation in control arterioles (max 179% +/− 27 control, 71% +/− 17 nano-TiO_2 (Figure 5C)), suggesting a COX-mediated compensation for the reduced NO bioavailability in the nano-TiO_2-exposed animals.

Nanoparticle inhalation alters sensitivity to COX products

Because the balance of vasoactive factors following AH appeared to be more dependent on a COX-mediated pathway after nano-TiO_2 exposure, the relative sensitivity of these arterioles to COX product mimetics was determined. Superfusion of the thromboxane A_2 (TxA_2) mimetic, U46619, led to a dose-dependent vasoconstrictive effect (Figure 6A). The overall vasoconstrictive effect of U46619 was greater in the nano-TiO_2-exposed animals at 1 nM compared with control, indicating a greater sensitivity to TxA_2 (Figure 6A). Conversely, the prostacyclin analogue iloprost led to a

Table II. Characteristics of all arterioles studied.

	Control			Nano-TiO_2		
Superfusate	*n*	Diameter (μm)	% Tone	*n*	Diameter (μm)	% Tone
Normal	59	34 ± 1	66 ± 1	71	34 ± 1	68 ± 1
L-NMMA	17	32 ± 2	65 ± 3	16	32 ± 2	69 ± 2
Meclofenamate	15	35 ± 3	68 ± 3	17	36 ± 2	66 ± 2
Phentolamine	18	30 ± 2	70 ± 2	23	41* ± 4	63* ± 3
Tetrodotoxin	4	29 ± 2	65 ± 3	9	31 ± 2	65 ± 4
Passive diameter	59	102 ± 2		71	107 ± 3	

*$p < 0.05$ vs. control arterioles; Data are means ± SE; *n* = number of vessels per group.

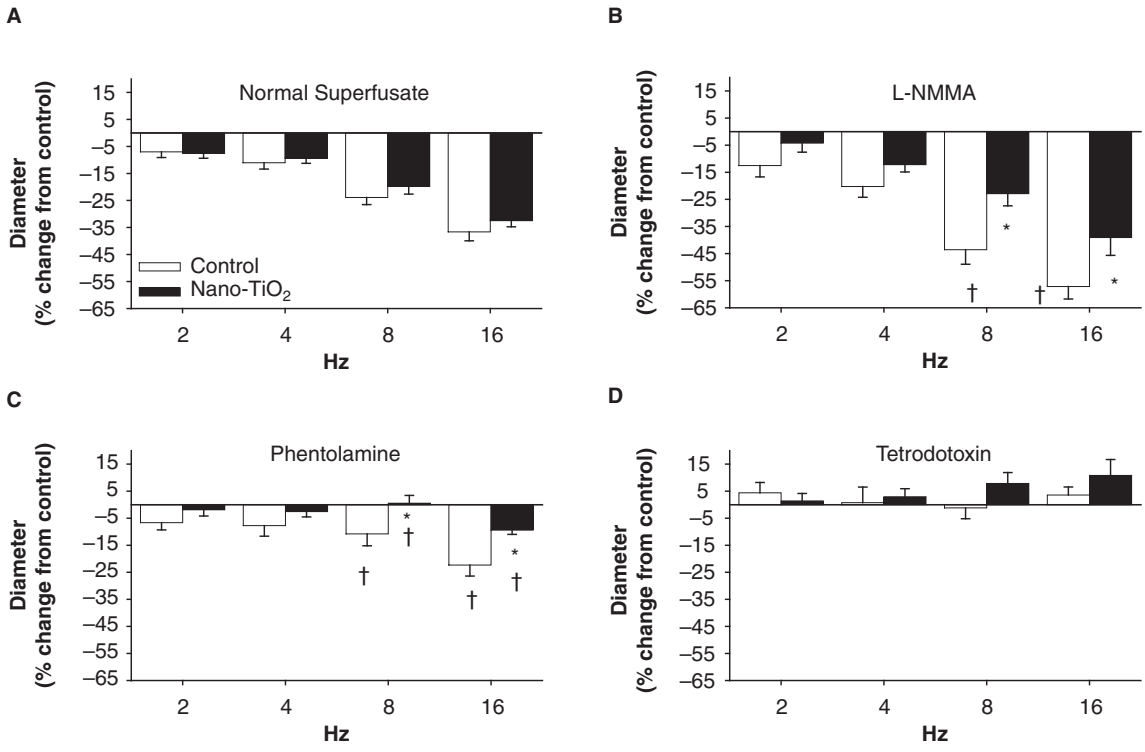

Figure 4. Nanoparticle inhalation alters arteriolar responsiveness to sympathetic stimulation following L-NMMA and phentolamine treatment. PVNS was performed as described in the Methods. (A) Nano-TiO_2 exposure did not alter responsiveness to sympathetic arteriole constriction during normal PSS superfusion ($n = 23$ control, 27 nano-TiO_2-exposed arterioles). (B) Treatment with L-NMMA increased arteriolar constriction in control animals but not nano-TiO_2-exposed animals ($n = 10$ control, 12 nano-TiO_2-exposed arterioles). (C) Nano-TiO_2 exposure increased sensitivity to α-adrenergic blockade during sympathetic arteriolar constriction ($n = 10$ control, 11 nano-TiO_2-exposed arterioles). (D) Tetrodotoxin significantly ablated arteriolar constriction in all groups ($n =$ four control, nine nano-TiO_2-exposed arterioles). Values are means ± SE. *$p < 0.05$ vs. control at same stimulation frequency, †$p < 0.05$ vs. normal superfusate at the same frequency.

dose-dependent vasodilatory effect (Figure 6B). There was a decrease in sensitivity to iloprost superfusion at 2.8 nM in the nano-TiO_2-exposed rats compared with control (Figure 6B). These data suggest that, in addition to a possible COX-product compensation for the lack of NO bioavailability, nanoparticle exposure also alters sensitivity to COX products.

Nanoparticle exposure induces persistent sympathetically mediated arteriolar dysfunction

Phentolamine superfusion led to a significant vasodilatory effect in the nano-TiO_2-exposed arterioles (Table II). However, AH-induced vasodilation at 12 Hz continued to be impaired even in the presence of α-adrenergic blockade following nano-TiO_2 exposure (Figure 7). These data suggest that even during α-adrenergic receptor inhibition or in the absence of sympathetic influence, nanoparticle exposure stimulates vasoactive influences that favour arteriolar constriction, and this effect cannot be overcome by local metabolic influences.

Discussion

Alterations in vascular reactivity following particle inhalation have been consistently demonstrated in the literature (Nurkiewicz et al. 2004; Mills et al. 2005; Rundell et al. 2007; Shah et al. 2008; LeBlanc et al. 2010). However, it remains unclear through what mechanism(s) these effects occur. The nanoparticle used in this study had minimal inherent pulmonary toxicity, as evidenced by no change in inflammatory proteins measured in bronchoalveolar lavage fluid and the relatively minor alveolar inflammation-induced following inhalation at total retained deposition of 10 μg (Nurkiewicz et al. 2008). Given the ubiquitous inclusion of TiO_2 in everyday products, this particle is relevant to both occupational (Madl & Pinkerton 2009) and personal exposures (Newman et al. 2009). Nano-TiO_2 exposure (1) augmented arteriolar α-adrenergic receptor sensitivity, (2) decreased the influence of NO on sympathetic nerve-mediated arteriolar constriction, (3) impaired arteriolar responsiveness to metabolic stimuli and (4) altered either the balance of or arteriolar sensitivity to COX products.

Similar to other vascular beds, sympathetic efferents project into the spinotrapezius microvasculature and terminate at approximately the third-order arcade arterioles (Todd 1980; Marshall 1982). We stimulated these neurons via PVNS to produce arteriolar constriction in a graduated manner that was frequency dependent (Figure 4). These arterioles exhibited sensitivity to α-adrenergic receptor antagonism following nanoparticle inhalation (Table II). This vasodilatory effect during α-adrenergic blockade suggests that an altered tonic sympathetic activity follows nanoparticle inhalation. It has been shown that at neurovascular junctions, neuropeptide Y, norepinephrine and perhaps ATP serve critical functions (Huidobro-Toro & Donoso 2004) and are important in sympathetic vasoconstriction (Coney & Marshall 2007).

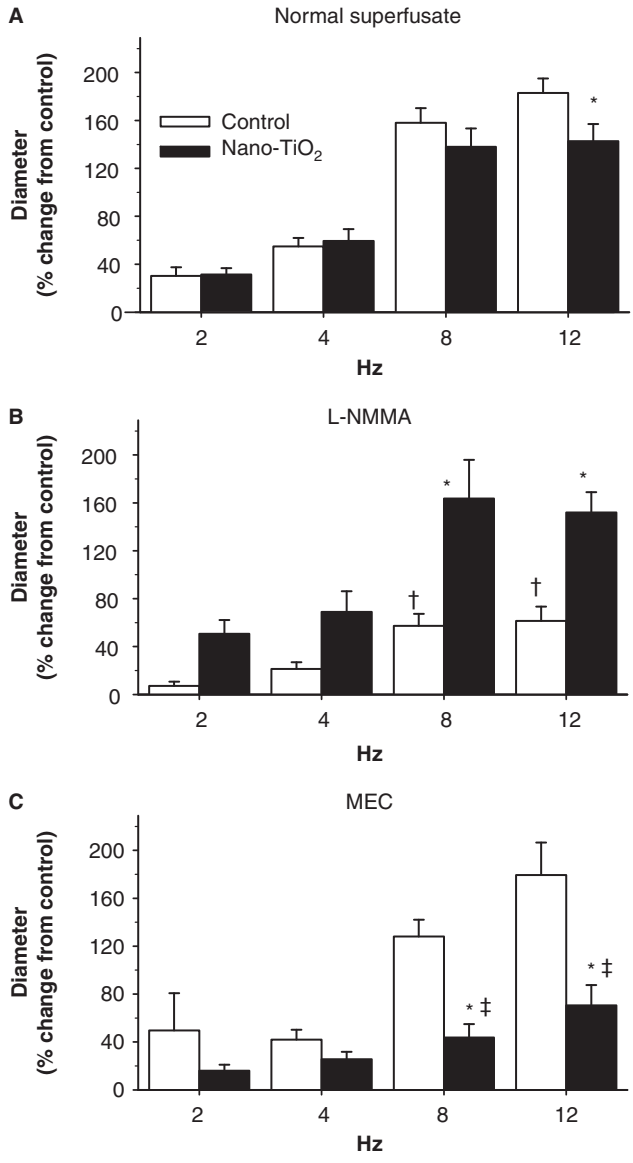

Figure 5. Nanoparticle inhalation attenuates functional arteriolar dilation during active hyperaemia. (A) Nano-TiO_2 exposure reduces arteriolar vasodilation to metabolic stimuli (n = 23 control, 31 nano-TiO_2-exposed arterioles). (B) Inhibition of NO production with N^G-monomethyl-l-arginine (L-NMMA) attenuates arteriolar dilation in control animals but not nano-TiO_2 exposed (n = eight control, nine nano-TiO_2-exposed arterioles). (C) Conversely, inhibition of cyclooxygenase impairs arteriolar dilation in nano-TiO_2-exposed animals compared with control (n = 9 control, 15 nano-TiO_2-exposed arterioles). MEC, meclofenamate. Values are means ± SE. $^*p < 0.05$ vs. control, $^\dagger p < 0.05$ vs. control normal superfusate at the same frequency, $^\ddagger p < 0.05$ vs. nano-TiO_2-exposed normal superfusate at the same frequency.

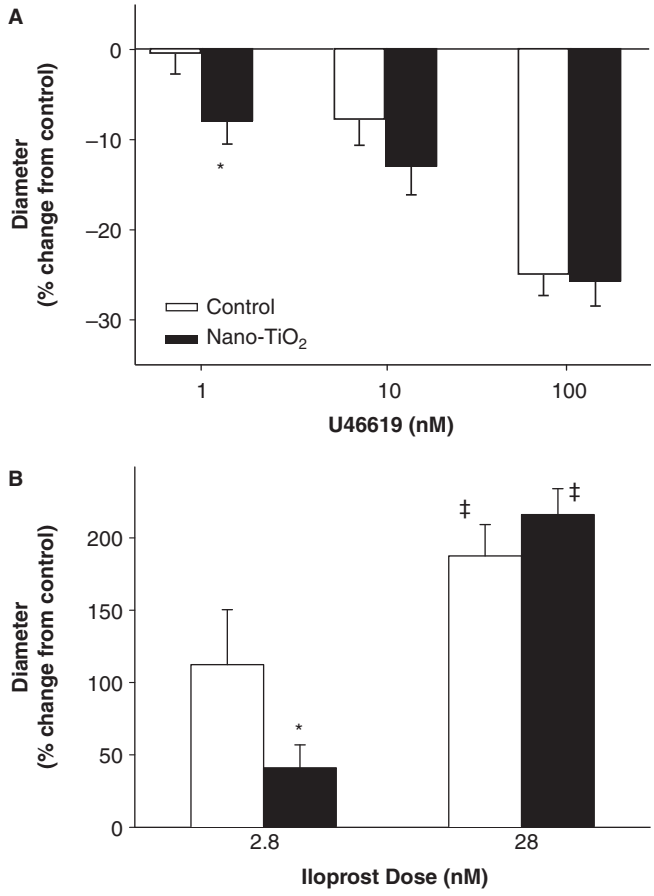

Figure 6. Pulmonary nanoparticle exposure alters arteriolar responsiveness to thromboxane A_2 (TxA_2) and prostacyclin mimetics. (A) Superfusion of the spinotrapezius muscle with U46619, a TxA_2 mimetic, significantly enhanced arteriolar constriction following nano-TiO_2 exposure compared with control animals at 1 nM (n = 16 control, 13 nano-TiO_2-exposed arterioles). (B) Iloprost superfusion led to a dose-dependent arteriolar dilation that was significantly blunted at 2.8 nM following nano-TiO_2 exposure (2.8 nM n = 9 control and n = 13 nano-TiO_2 exposed; 28 nM n = 11 control and n = 16 nano-TiO_2-exposed arterioles). Values are means ± SE. $^*p < 0.05$ vs. control exposure, $^\ddagger p < 0.05$ vs. 2.8 nM iloprost.

Additionally, the enhanced sensitivity in nanoparticle exposed animals to α-adrenergic receptor blockade during PVNS (Figure 4C) may suggest a predominance of norepinephrine-mediated constriction.

Several studies have demonstrated a reduction in NO bioavailability in humans (Mills et al. 2005; Tornqvist et al. 2007; Shah et al. 2008) and in animal toxicological studies (Nurkiewicz et al. 2006; Proctor et al. 2006; Knuckles et al. 2008). Basal arteriolar tone was not altered following superfusion with L-NMMA in control or nanoparticle-exposed animals (Table II), which is not surprising given the multitude of extrinsic and intrinsic signals that regulate basal tone (Segal 2005). PVNS stimulation in the presence of the NOS inhibitor L-NMMA enhanced arteriolar constriction in control animals while not altering the responses in nanoparticle-exposed animals (Figure 4B). Similarly, inhibition of NOS activity blunted the hyperaemia-induced arteriolar dilation in control animals while not affecting arterioles from nanoparticle-exposed animals (Figure 5B). These data are consistent with previous reports that bioavailable NO reduces arteriolar constriction during PVNS (Linderman & Boegehold 1998) and is an important mediator of hyperaemia-induced vasodilation (Dua et al. 2009).

As discussed above, loss of NO bioavailability has been explored extensively in human and animal models either through endothelium-dependent or endothelium-independent mechanisms (Mills et al. 2005; Campen et al. 2005; Rundell et al. 2007; Knuckles et al. 2008; Shah et al. 2008; Cherng et al. 2009; Nurkiewicz et al. 2009). Furthermore, previous work by our laboratory and others has shown a consistent attenuation in both humans and animals of NO

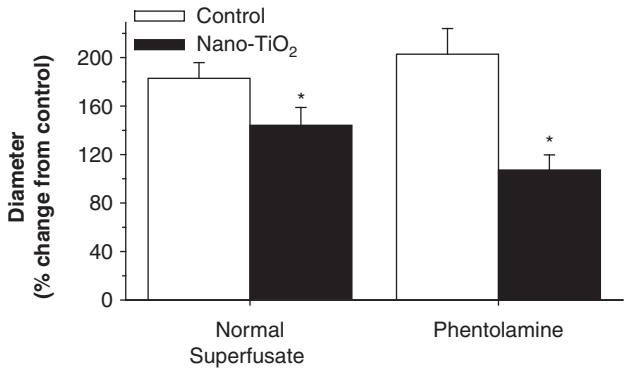

Figure 7. Nanoparticle inhalation exposure resulted in persistent blunting of arteriolar dilation without the influence of sympathetic nerves. α-Adrenergic blockade failed to alter the blunting of arteriolar dilation following active hyperaemia at 12 Hz in nano-TiO_2-exposed animals. Values are means ± SE. *$p < 0.05$ vs. control exposure.

bioavailability following inhalation of particles that is likely reactive oxygen species related (Nurkiewicz et al. 2004; Mills et al. 2005; Nurkiewicz et al. 2006; Knuckles et al. 2008; Nurkiewicz et al. 2009; Cherng et al. 2011). Other mechanisms of vasodilation have not been as vigorously explored. However, obviously vascular function, however blunted, still exists. In humans, Mills et al. (2005) showed that relative vasoreactivity in arteries was altered to a range of mechanistically distinct compounds. Specifically, Mills and colleagues determined deficits in vasodilation following bradykinin, acetylcholine and sodium nitroprusside. These data highlight both a deficit in production of NO as well as utilisation of NO. Hence, the overall consensus of their work and others is that fine particles, nanoparticles or air pollutants limit vasodilation through reductions in NO bioavailability.

While several lines of evidence have demonstrated reductions in NO following particle exposure, none has shown a link between sympathetic influence and vascular function. Within the literature, limited data exist for altered sympathetic influence in the vasculature following particle exposure. Our laboratory was the first to report that inhibition of fast Na^+ channels with tetrodotoxin partially restores endothelium-dependent arteriolar dilation in nano-TiO_2-exposed rats (Nurkiewicz et al. 2011). Within the broader literature, alterations in autonomic nervous system function (i.e. parasympathetic and sympathetic) have been largely confined to measures of heart rate variability (HRV). While these measures are essential in humans, their translation in rodent models is less clear, given the indirect nature of the measurement and the lack of testable mechanistic outcomes (Rowan, III et al. 2007).

While autonomic nervous system data with HRV measures can be difficult to interpret in animal studies, several epidemiological and clinical studies have clearly shown an increase in blood pressure following PM exposure (Brook et al. 2009; Liu et al. 2009). Furthermore, the increase in arterial blood pressure in both human and animal models appears to be diastolic in origin (Zanobetti et al. 2004; Bartoli et al. 2009; Brook et al. 2009). In a dog model, Bartoli et al. (2009) found that the transient increases in blood pressure could be mitigated with the systemic addition of an α-adrenergic receptor blocker, prazosin, during PM exposure. Furthermore, the PM-exposed dogs had an altered baroreceptor reflex response compared with control. PM exposure also led to a prolongation of the R–R interval relative to increase in systolic blood pressure following transient infusion of phenylephrine. These data suggest that the origin of the increased blood pressure following particle inhalation is likely sympathetic. Furthermore, the increase in diastolic pressure indicates an increase in arteriolar resistance (Stouffer 2008). In our study, while baseline arteriolar diameters and tone were not altered under the normal superfusate condition between exposure groups, α-adrenergic blockade resulted in a significant dilation in the nanoparticle-exposed group (Table II). This suggests an increase in tonic sympathetic influence in our study that is consistent with results found by Bartoli et al. (2009). Furthermore, we hypothesise that based on the reported increases in diastolic blood pressure and the changes in tonic sympathetic influence, blood pressure would be altered in our animals following nanoparticle exposure. Our mean arterial pressure (MAP), systolic blood pressure (SBP), diastolic blood pressure (DBP) and heart rate (HR) measurements were different between control and nanoparticle exposed animals (Table I). However, it is not clear whether the effect was the result of the rats in the nanoparticle-exposed group having a larger mass and hence a slightly greater blood pressure and heart rate or an effect of nanoparticle exposure. The intravital microscopy technique employed in this study requires the use of anaesthesia, which makes it difficult to confidently extrapolate any differences in blood pressure and heart rate between groups. Future studies will incorporate arterial blood pressure measurements in telemetered conscious animals to determine whether nanoparticle inhalation exposure increases blood pressure.

In this study, we found that AH-induced vasodilation was significantly attenuated after nanoparticle inhalation. This suggests an alteration in the sensitivity, production or uptake of vasoactive metabolites, which may be partially due to a reduction in NO bioavailability. Further study revealed that the compensatory mechanism for this apparent loss in NO bioavailability is probably COX-mediated (Figure 5C). Furthermore, α-adrenergic blockade, while resulting in a vasodilatory effect at baseline (Table II), failed to normalise vasodilation to AH (Figure 7). While we expected α-adrenergic blockade to normalise AH-induced arteriolar dilation in the nanoparticle-exposed animals, an alternative explanation for the lack of normalisation would be that the effects of adrenergic stimulation continue to impair vasodilation even in the absence of new adrenergic signalling. Previous work by Faber & Meininger (1990) demonstrated that pre-exposure to adrenergic agonists predisposed tissues to hyperconstriction and led to a greater resistance to vasodilation even in the absence of changes in arteriolar tone (Faber & Meininger 1990). In the context of the present study, nanoparticle inhalation appears to enhance sympathetic influence, which is through an adrenergic pathway (Table II, Figure 4C). Hence, these data support a

predisposition towards vasoconstriction via an adrenergic mechanism, since α-adrenergic receptor antagonism failed to normalise metabolically induced vasodilation (Figure 7). Additionally, peroxynitrite, which is increased following nano-TiO_2 exposure (Nurkiewicz et al. 2008), has been shown to increase RhoA/Rho kinase activity (El-Remessy et al. 2010), which promotes calcium sensitivity in resistance arterioles (Bolz et al. 2003). The enhanced calcium sensitivity may play a role in the persistent attenuation of vasodilation observed following phentolamine treatment and AH-mediated vasodilation in nanoparticle-exposed animals (Figure 7). Furthermore, this is consistent with an augmented responsiveness to the calcium ionophore, A23187, following exposure to nanoparticles (Nurkiewicz et al. 2008; LeBlanc et al. 2009; Nurkiewicz et al. 2009).

TxA_2 is a potent vasoconstrictor and one of several metabolites of arachidonic acid that has been shown to play a significant role in platelet aggregation, bronchoconstriction and vasoconstriction (Dogne et al. 2004), as well as microvascular dysfunction (Goodwill et al. 2008a, 2008b). Increased sensitivity to TxA_2 can occur through increased receptor density (Dogne et al. 2004) as well as decreases in the formation of antagonistic arachidonic acid metabolites (Goodwill et al. 2008b). Some hallmarks of increased TxA_2 sensitivity have been shown in context to PM and nanoparticle exposures (e.g. enhanced vasoconstriction (Brook et al. 2002; Rundell et al. 2007), and platelet aggregation (Nemmar et al. 2008)). There appears to be an enhanced sensitivity to TxA_2 and a reduction in sensitivity to prostacyclin possibly leading to an overall pro-constrictive effect for COX mimetics following nanoparticle exposure (Figure 6). Hillslope analysis suggests a right-shifted EC_{50} curve following exposure to nanoparticles (data not shown), but the biological relevance of this effect is unclear at this time. Moreover, the vasoreactivity data to COX mimetics should be interpreted with caution because a full dose range should be developed in future studies. Collectively, these data suggest an altered production of COX metabolites (Figure 5C) as well as altered prostanoid receptor activity, distribution and/or signalling mechanisms (Figure 6). Future studies should also determine the role of nanoparticle inhalation in altering COX product formation, prostanoid receptor distribution and alterations in COX isoform expression.

The reduction in NO bioavailability highlighted in this work, and previously demonstrated in this vascular bed following nanoparticle exposure (Nurkiewicz et al. 2009), appears to be compensated for through a shift to a COX-mediated mechanism. Previous work by LeBlanc et al. (2010) demonstrated in isolated coronary arterioles that nanoparticle inhalation exposure led to a slight vasoconstriction to arachidonic acid (the metabolic precursor to prostacyclin and TxA_2), whereas control arterioles exhibited vasodilation. Nanoparticle exposure did not alter vasoconstriction to U46619. Furthermore, coronary arteriolar endothelium-dependent vasodilation with acetylcholine following nanoparticle inhalation exposure was attenuated compared with control animals (LeBlanc et al. 2009, 2010). However, the addition of L-NMMA or indomethacin (a preferential COX-1 inhibitor) did not alter vasodilation in the nanoparticle-exposed animals (LeBlanc et al. 2010). While not a complete investigation, these data in isolated coronary arterioles suggest that inhaled nanoparticles alter arteriolar vasoreactivity correspondingly across different vascular beds. Furthermore, flow-mediated dilation was nearly normal in coronary arterioles isolated from nanoparticle-exposed rat compared with control (LeBlanc et al. 2009). These data suggest that while impairments in NO-mediated vasodilation are present, compensatory mechanisms (e.g. COX products), or a shift in their contributions, at least partially preserve the functional vasoreactivity following nanoparticle exposure.

The dose relationship of these exposures in humans was highlighted in Nurkiewicz et al. (2009). Briefly, the occupational limit for fine TiO_2 is 5 mg/m^3. Measured levels of nano-TiO_2 in a production plant are as high as 1.4 $\mu g/m^3$. Thus, an equivalent pulmonary burden in human to 10 μg in the rat would be achieved in roughly 5 years (Nurkiewicz et al. 2009).

This study demonstrates that nanoparticle inhalation negatively impacts arteriolar tone and reactivity via mechanisms that are not exclusively endothelium-dependent. These data also highlight a reduction in responsiveness to metabolic stimuli as well as an altered tonic sympathetic influence. Furthermore, the normal vasodilatory NO signal is blunted following nanoparticle exposure, which is likely compensated for through a COX-mediated pathway. This study also highlights the need for a greater understanding of the complex changes in vascular physiology that result from particle exposure. While the effects of particle exposure on vascular reactivity have been largely described through a reduction in NO bioavailability, generation of vascular resistance is a mechanistically complex interplay of a variety of influences and will require continued comprehensive investigations of all avenues of vasoregulation. Future studies should focus on measuring sympathetic nerve activity following exposure to nanoparticles, as well as using therapeutic interventions to prevent nanoparticle-induced microvascular dysfunction.

Acknowledgements

The authors would like to thank Carroll McBride and Kimberly Wix for their expert technical assistance in this study. We also thank Phoebe Stapleton, Ph.D., for her critical review of the manuscript. The authors would also like to thank Michael McCawley, Ph.D., for his expert technical assistance with modelling the particle distributions. Funding sources: RO-1 ES015022 and RC-1 ES018274 (TRN). *Disclaimer: The findings and conclusions in this article are those of the authors and do not necessarily represent the view of the National Institute for Occupational Safety and Health.*

Declaration of interest

The author reports no conflicts of interest. The author alone is responsible for the content and writing of the paper.

References

Aitken RJ, Chaudhry MQ, Boxall AB, Hull M. 2006. Manufacture and use of nanomaterials: current status in the UK and global trends. Occup Med (Lond) 56:300–306.

Bartoli CR, Wellenius GA, Diaz EA, Lawrence J, Coull BA, Akiyama I, et al. 2009. Mechanisms of inhaled fine particulate air pollution-induced arterial blood pressure changes. Environ Health Perspect 117:361–366.

Boegehold MA. 1991. Effect of salt-induced hypertension on microvascular pressures in skeletal muscle of Dahl rats. Am J Physiol 260: H1819–H1825.

Boegehold MA, Bohlen HG. 1988. Arteriolar diameter and tissue oxygen tension during muscle contraction in hypertensive rats. Hypertension 12:184–191.

Bolz SS, Vogel L, Sollinger D, Derwand R, De WC, Loirand G, Pohl U. 2003. Nitric oxide-induced decrease in calcium sensitivity of resistance arteries is attributable to activation of the myosin light chain phosphatase and antagonized by the RhoA/Rho kinase pathway. Circulation 107:3081–3087.

Brook RD, Brook JR, Urch B, Vincent R, Rajagopalan S, Silverman F. 2002. Inhalation of fine particulate air pollution and ozone causes acute arterial vasoconstriction in healthy adults. Circulation 105:1534–1536.

Brook RD, Urch B, Dvonch JT, Bard RL, Speck M, Keeler G, et al. 2009. Insights into the mechanisms and mediators of the effects of air pollution exposure on blood pressure and vascular function in healthy humans. Hypertension 54:659–667.

Campen MJ, Babu NS, Helms GA, Pett S, Wernly J, Mehran R, McDonald JD. 2005. Nonparticulate components of diesel exhaust promote constriction in coronary arteries from ApoE-/- mice. Toxicol Sci 88:95–102.

Cherng TW, Campen MJ, Knuckles TL, Gonzalez BL, Kanagy NL. 2009. Impairment of coronary endothelial cell ET(B) receptor function after short-term inhalation exposure to whole diesel emissions. Am J Physiol Regul Integr Comp Physiol 297:R640–R647.

Cherng TW, Jackson-Weaver O, Paffett M, walker B, Campen MJ, Kanagy NL. 2011. Mechanisms of diesel-induced endothelial NOS dysfunction in coronary arterioles. Environ Health Persp 119:98–103.

Coney AM, Marshall JM. 2007. Contribution of alpha2-adrenoceptors and Y1 neuropeptide Y receptors to the blunting of sympathetic vasoconstriction induced by systemic hypoxia in the rat. J Physiol 582:1349–1359.

Didion SP, Carmines PK, Ikenaga H, Mayhan WG. 1997. Enhanced constrictor responses of skeletal muscle arterioles during chronic myocardial infarction. Am J Physiol 273:H1502–H1508.

Dogne JM, De Leval X, Hanson J, Frederich M, Lambermont B, Ghuysen A, et al. 2004. New developments on thromboxane and prostacyclin modulators part I: thromboxane modulators. Curr Med Chem 11:1223–1241.

Dreher KL, Jaskot RH, Lehmann JR, Richards JH, McGee JK, Ghio AJ, Costa DL. 1997. Soluble transition metals mediate residual oil fly ash induced acute lung injury. J Toxicol Environ Health 50:285–305.

Dua AK, Dua N, Murrant CL. 2009. Skeletal muscle contraction-induced vasodilator complement production is dependent on stimulus and contraction frequency. Am J Physiol Heart Circ Physiol 297: H433–H442.

El-Remessy AB, Tawfik HE, Matragoon S, Pillai B, Caldwell RB, Caldwell RW. 2010. Peroxynitrite mediates diabetes-induced endothelial dysfunction: possible role of Rho kinase activation. Exp Diabetes Res 2010:247861.

Faber JE, Meininger GA. 1990. Selective interaction of alpha-adrenoceptors with myogenic regulation of microvascular smooth muscle. Am J Physiol 259:H1126–H1133.

Goodwill AG, James ME, Frisbee JC. 2008a. Increased vascular thromboxane generation impairs dilation of skeletal muscle arterioles of obese zucker rats with reduced oxygen tension. Am J Physiol Heart Circ Physiol 295:H1522–H1528.

Goodwill AG, Stapleton PA, James ME, D'Audiffret AC, Frisbee JC. 2008b. Increased arachidonic acid-induced thromboxane generation impairs skeletal muscle arteriolar dilation with genetic dyslipidemia. Microcirculation 15:621–631.

Huidobro-Toro PJ, Donoso V. 2004. Sympathetic co-transmission: the coordinated action of ATP and noradrenaline and their modulation by neuropeptide Y in human vascular neuroeffector junctions. Eur J Pharmacol 500:27–35.

Knuckles TL, Lund AK, Lucas SN, Campen MJ. 2008. Diesel exhaust exposure enhances venoconstriction via uncoupling of eNOS. Toxicol Appl Pharmacol 230:346–51.

Kurjiaka DT, Segal SS. 1995. Interaction between conducted vasodilation and sympathetic nerve activation in arterioles of hamster striated muscle. Circ Res 76:885–891.

Lash JM. 1995. Arterial and arteriolar contributions to skeletal muscle functional hyperemia in spontaneously hypertensive rats. J Appl Physiol 78:93–100.

Lash JM, Bohlen HG. 1987. Perivascular and tissue PO2 in contracting rat spinotrapezius muscle. Am J Physiol 252:H1192–H1202.

LeBlanc AJ, Cumpston JL, Chen BT, Frazer D, Castranova V, Nurkiewicz TR. 2009. Nanoparticle inhalation impairs endothelium-dependent vasodilation in subepicardial arterioles. J Toxicol Environ Health A 72:1576–1584.

LeBlanc AJ, Moseley AM, Chen BT, Frazer D, Castranova V, Nurkiewicz TR. 2010. Nanoparticle inhalation impairs coronary microvascular reactivity via a local reactive oxygen species-dependent mechanism. Cardiovasc Toxicol 10:27–36.

Linderman JR, Boegehold MA. 1998. Modulation of arteriolar sympathetic constriction by local nitric oxide: onset during rapid juvenile growth. Microvasc Res 56:192–202.

Liu L, Ruddy T, Dalipaj M, Poon R, Szyszkowicz M, You H, et al. 2009. Effects of indoor, outdoor, and personal exposure to particulate air pollution on cardiovascular physiology and systemic mediators in seniors. J Occup Environ Med 51:1088–1098.

Madl AK, Pinkerton KE. 2009. Health effects of inhaled engineered and incidental nanoparticles. Crit Rev Toxicol 39:629–658.

Marshall JM. 1982. The influence of the sympathetic nervous system on individual vessels of the microcirculation of skeletal muscle of the rat. J Physiol 332:169–186.

Marvar PJ, Nurkiewicz TR, Boegehold MA. 2005. Reduced arteriolar responses to skeletal muscle contraction after ingestion of a high salt diet. J Vasc Res 42:226–236.

Maynard AD, Aitken RJ, Butz T, Colvin V, Donaldson K, Oberdorster G, et al. 2006. Safe handling of nanotechnology. Nature 444:267–269.

Mills NL, Tornqvist H, Robinson SD, Gonzalez M, Darnley K, MacNee W, et al. 2005. Diesel exhaust inhalation causes vascular dysfunction and impaired endogenous fibrinolysis. Circulation 112:3930–3936.

Nase GP, Boegehold MA. 1997a. Endothelium-derived nitric oxide limits sympathetic neurogenic constriction in intestinal microcirculation. Am J Physiol 273:H426–H433.

Nase GP, Boegehold MA. 1997b. Modulation of sympathetic constriction by the arteriolar endothelium does not involve the cyclooxygenase pathway. Int J Microcirc Clin Exp 17:41–47.

Nemmar A, Melghit K, Ali BH. 2008. The acute proinflammatory and prothrombotic effects of pulmonary exposure to rutile TiO2 nanorods in rats. Exp Biol Med (Maywood) 233:610–619.

Newman MD, Stotland M, Ellis JI. 2009. The safety of nanosized particles in titanium dioxide- and zinc oxide-based sunscreens. J Am Acad Dermatol 61:685–692.

Nurkiewicz TR, Porter DW, Barger M, Castranova V, Boegehold MA. 2004. Particulate matter exposure impairs systemic microvascular endothelium-dependent dilation. Environ Health Perspect 112:1299–1306.

Nurkiewicz TR, Porter DW, Barger M, Millecchia L, Rao KM, Marvar PJ, et al. 2006. Systemic microvascular dysfunction and inflammation after pulmonary particulate matter exposure. Environ Health Perspect 114:412–419.

Nurkiewicz TR, Porter DW, Hubbs AF, Cumpston JL, Chen BT, Frazer DG, Castranova V. 2008. Nanoparticle inhalation augments particle-dependent systemic microvascular dysfunction. Part Fibre Toxicol 5:1.

Nurkiewicz TR, Porter DW, Hubbs AF, Stone S, Chen BT, Frazer DG, et al. 2009. Pulmonary nanoparticle exposure disrupts systemic microvascular nitric oxide signaling. Toxicol Sci 110:191–203.

Nurkiewicz TR, Porter DW, Hubbs AF, Stone S, Moseley AM, Cumpston JL, et al. 2011. Pulmonary particulate matter and systemic microvascular dysfunction. Res Rep Health Eff Inst.

Oberdorster G, Sharp Z, Atudorei V, Elder A, Gelein R, Kreyling W, Cox C. 2004. Translocation of inhaled ultrafine particles to the brain. Inhal Toxicol 16:437–445.

Proctor SD, Dreher KL, Kelly SE, Russell JC. 2006. Hypersensitivity of prediabetic JCR:LA-cp rats to fine airborne combustion

particle-induced direct and noradrenergic-mediated vascular contraction. Toxicol Sci 90:385–391.
Rowan WH, III, Campen MJ, Wichers LB, Watkinson WP. 2007. Heart rate variability in rodents: uses and caveats in toxicological studies. Cardiovasc Toxicol 7:28–51.
Rundell KW, Hoffman JR, Caviston R, Bulbulian R, Hollenbach AM. 2007. Inhalation of ultrafine and fine particulate matter disrupts systemic vascular function. Inhal Toxicol 19:133–140.
Sager TM, Castranova V. 2009. Surface area of particle administered versus mass in determining the pulmonary toxicity of ultrafine and fine carbon black: comparison to ultrafine titanium dioxide. Part Fibre Toxicol 6:15.
Sager TM, Kommineni C, Castranova V. 2008. Pulmonary response to intratracheal instillation of ultrafine versus fine titanium dioxide: role of particle surface area. Part Fibre Toxicol 5:17.
Schmid-Schonbein GW, Skalak R, Chien S. 1991. Hemodynamics in arteriolar networks. In: Bevan JA, Halpren W, Mulvany MJ, editors. The Resistance Vasculature. Humana Press. pp 319–344.
Segal SS. 2005. Regulation of blood flow in the microcirculation. Microcirculation 12:33–45.
Shah AP, Pietropaoli AP, Frasier LM, Speers DM, Chalupa DC, Delehanty JM, et al. 2008. Effect of inhaled carbon ultrafine particles on reactive hyperemia in healthy human subjects. Environ Health Perspect 116:375–380.
Shieh KJ, Li M, Lee YH, Sheu SD, Liu YT, Wang YC. 2006. Antibacterial performance of photocatalyst thin film fabricated by defection effect in visible light. Nanomedicine 2:121–126.
Stone PH, Godleski JJ. 1999. First steps toward understanding the pathophysiologic link between air pollution and cardiac mortality. Am Heart J 138:804–807.
Stone V, Johnston H, Clift MJ. 2007. Air pollution, ultrafine and nanoparticle toxicology: cellular and molecular interactions. IEEE Trans Nanobioscience 6:331–340.
Stouffer GA. 2008. Cardiovascular Hemodynamics for the Clinician. John Wiley and Sons. p 59.
Sun D, Meng TT, Loong TH, Hwa TJ. 2004. Removal of natural organic matter from water using a nano-structured photocatalyst coupled with filtration membrane. Water Sci Technol 49:103–110.
Tamagawa E, Bai N, Morimoto K, Gray C, Mui T, Yatera K, et al. 2008. Particulate matter exposure induces persistent lung inflammation and endothelial dysfunction. Am J Physiol Lung Cell Mol Physiol 295:L79–L85.
Todd ME. 1980. Development of adrenergic innervation in rat peripheral vessels: a fluorescence microscopic study. J Anat 131:121–133.
Tornqvist H, Mills NL, Gonzalez M, Miller MR, Robinson SD, Megson IL, et al. 2007. Persistent endothelial dysfunction in humans after diesel exhaust inhalation. Am J Respir Crit Care Med 176:395–400.
Vicaut E. 1999. Microcirculation and arterial hypertension. Drugs 59:1–10.
Xiang L, Naik JS, Hodnett BL, Hester RL. 2006. Altered arachidonic acid metabolism impairs functional vasodilation in metabolic syndrome. Am J Physiol Regul Integr Comp Physiol 290:R134–R138.
Zanobetti A, Canner MJ, Stone PH, Schwartz J, Sher D, Eagan-Bengston E, et al. 2004. Ambient pollution and blood pressure in cardiac rehabilitation patients. Circulation 110:2184–2189.